TECHNICAL REPORTS

nature medicine

Enhancing the precision of genetic lineage tracing using dual recombinases

Lingjuan He[1,2], Yan Li[1,2], Yi Li[1,2], Wenjuan Pu[1,2], Xiuzhen Huang[1,2], Xueying Tian[1,2], Yue Wang[1,2], Hui Zhang[1,2], Qiaozhen Liu[1,2], Libo Zhang[1,2], Huan Zhao[1,2], Juan Tang[1,2], Hongbin Ji[1,3], Dongqing Cai[4], Zhibo Han[5], Zhongchao Han[5], Yu Nie[6], Shengshou Hu[6], Qing-Dong Wang[7], Ruilin Sun[8], Jian Fei[8], Fengchao Wang[9], Ting Chen[9], Yan Yan[10], Hefeng Huang[11], William T Pu[12] & Bin Zhou[1–4,13]

The Cre–*loxP* recombination system is the most widely used technology for *in vivo* tracing of stem or progenitor cell lineages. The precision of this genetic system largely depends on the specificity of Cre recombinase expression in targeted stem or progenitor cells. However, Cre expression in nontargeted cell types can complicate the interpretation of lineage-tracing studies and has caused controversy in many previous studies. Here we describe a new genetic lineage tracing system that incorporates the Dre–*rox* recombination system to enhance the precision of conventional Cre–*loxP*-mediated lineage tracing. The Dre–*rox* system permits rigorous control of Cre–*loxP* recombination in lineage tracing, effectively circumventing potential uncertainty of the cell-type specificity of Cre expression. Using this new system we investigated two topics of recent debates—the contribution of c-Kit$^+$ cardiac stem cells to cardiomyocytes in the heart and the contribution of Sox9$^+$ hepatic progenitor cells to hepatocytes in the liver. By overcoming the technical hurdle of nonspecific Cre–*loxP*-mediated recombination, this new technology provides more precise analysis of cell lineage and fate decisions and facilitates the *in vivo* study of stem and progenitor cell plasticity in disease and regeneration.

During the process of differentiation, stem and progenitor cells make lineage choices that progressively narrow the range of cell types that can be generated, until the ultimate, differentiated cell type is formed. A cell's lineage captures its developmental trajectory from its progenitors, and a cell's fate is the differentiated cell type(s) that it will form. Unraveling cell lineage and fate determination provides fundamental information about stem cell function during development, disease and regeneration. Genetic lineage tracing is a powerful means to interrogate stem cell lineage and cell fate determination[1–6]. The most widely used technology for *in vivo* stem cell tracking uses the Cre–*loxP* recombination system[7]. In transgenic mice that express Cre within a defined population of stem cells, Cre-mediated recombination removes *loxP*-flanked transcriptional stop DNA sequences and permits expression of a reporter gene in the Cre$^+$ cells[8]. Because this form of genetic labeling is irreversible and heritable, the progeny of the Cre-marked cells continue to express the reporter gene, whether or not they actively express Cre. If a Cre-marked cell differentiates into a different cell type, then its expression of the genetic lineage reporter provides evidence that it belongs to the Cre-expressing lineage (**Fig. 1a**, scenario 1, cell type B (cell B) is derived from cell type A (cell A)).

Although Cre–*loxP*-based lineage tracing has provided unprecedented insights into mammalian development and into disease states, this technology has a technical hurdle that may sometimes confound interpretation of the results. The linchpin for accurate interpretation of Cre–*loxP*-based fate-mapping data is precise delineation of the pattern of Cre expression[9,10], as Cre expression in nontargeted cells could lead to the tracing of unintended lineages and confound interpretation of the fate-mapping data. For example, expression of a gene in both cell A and cell B can and often does occur. Cre labeling of both cell A and cell B cannot be used to formally conclude that cell A differentiates into cell B. Rather, this type of double labeling simply makes the genetic lineage tracing experiment uninterpretable. To properly infer that cell B is derived from cell A, one must exclude Cre–*loxP* recombination in cell B itself (**Fig. 1a**, scenario 2, in which the inference that cell B arises from cell A is confounded by Cre expression in cell B). Because Cre–*loxP*-mediated recombination is

[1]State Key Laboratory of Cell Biology, CAS Center for Excellence in Molecular Cell Science, Shanghai Institute of Biochemistry and Cell Biology, Chinese Academy of Sciences (CAS), University of Chinese Academy of Sciences, Shanghai, China. [2]Key Laboratory of Nutrition and Metabolism, Institute for Nutritional Sciences, Shanghai Institutes for Biological Sciences, Chinese Academy of Sciences, University of Chinese Academy of Sciences, Shanghai, China. [3]School of Life Science and Technology, ShanghaiTech University, Shanghai, China. [4]Key Laboratory of Regenerative Medicine of Ministry of Education, Institute of Aging and Regenerative Medicine, Jinan University, Guangzhou, China. [5]State Key Laboratory of Experimental Hematology, Institute of Hematology and Hospital of Blood Disease, Chinese Academy of Medical Science and Peking Union Medical College, Tianjin, China. [6]State Key Laboratory of Cardiovascular Disease, Fuwai Hospital, National Center for Cardiovascular Disease, Chinese Academy of Medical Sciences and Peking Union Medical College, Beijing, China. [7]Bioscience Heart Failure, Cardiovascular and Metabolic Diseases, IMED Biotech Unit, AstraZeneca, Gothenburg, Sweden. [8]Shanghai Model Organisms Center, Inc., Shanghai, China. [9]National Institute of Biological Sciences, Beijing, China. [10]Zhongshan Hospital, Fudan University, Shanghai, China. [11]International Peace Maternity and Child Health Hospital, School of Medicine, Shanghai Jiao Tong University, Shanghai, China. [12]Department of Cardiology, Boston Children's Hospital, Boston, Massachusetts, USA and Harvard Stem Cell Institute, Harvard University, Cambridge, Massachusetts, USA. [13]Collaborative Innovation Center of Tianjin for Medical Epigenetics, Tianjin Medical University, Tianjin, China. Correspondence should be addressed to B.Z. (zhoubin@sibs.ac.cn).

Received 1 March; accepted 11 October; published online 13 November 2017; doi:10.1038/nm.4437

sensitive, it can be technically challenging to fully exclude low level or infrequent Cre expression in nontargeted cells, creating a major hurdle for rigorous interpretation of the results of Cre–*loxP*-mediated genetic lineage tracing[10]. Here we present a new system that uses dual recombinases (Cre and Dre) and new reporter lines to resolve the unintentional lineage tracing issue and achieve more selective genetic tracing.

RESULTS

Generation of an interleaved dual reporter for exclusive recombination

To exclude genetic recombination in nontargeted cells, we generated a new genetic lineage tracing system that uses both the Cre–*loxP* and Dre–*rox* recombination systems. Similar to the Cre–*loxP* system, the Dre recombinase excises DNA regions flanked by *rox* recombination sites[11]. We first used mice that expressed these recombinases from the promoter of the widely expressed β-actin-expressing gene *ACTB* or from the synthetic promoter *CAG* (*ACTB–Cre* and *CAG–Dre*). We tested the activity and specificity of these transgenic mice using the recombinase-activated reporters *R26–loxP-tdTomato* (*R26–loxP–stop–loxP–tdTomato*) and *R26–rox–tdTomato* (*R26–rox–stop–rox–tdTomato*). We found that the Cre and Dre recombinases specifically recognized the *loxP* and *rox* sites, respectively (**Fig. 1b**), consistent with a previous report[12]. We took advantage of these orthogonal recombination systems and generated a reporter allele in the *Rosa26* locus in which two pairs of recombination recognition sites were interleaved, such that successful Cre–*loxP* recombination would activate expression of the ZsGreen reporter, whereas successful Dre–*rox* recombination would activate expression of the tdTomato reporter (**Fig. 1c**). We named this interleaved reporter (IR)-expressing mouse line IR1. Because the recombinase-recognition sites are interleaved (*loxP–rox–loxP–rox*), recombination by one system should inherently remove one recombinase-recognition site of the other system to render its reporter inert to subsequent recombination (for example, recombination using *Dre–rox* should remove one *loxP* site and prevent subsequent Cre–*loxP*-mediated recombination). Thus, in **Figure 1a**, scenario 2, programing cell B to express Dre first would preclude subsequent Cre–*loxP*-mediated recombination within this cell type.

To test this dual recombination system, we crossed the IR1 mouse line with lines that constitutively expressed Dre (*CAG–Dre*) or Cre (*ACTB–Cre*) (**Fig. 1d**). As expected by IR1's design, whole-mount fluorescence and immunostaining of sections showed that expression of tdTomato but not of ZsGreen was activated in the *CAG–Dre* × IR1 mice, whereas expression of ZsGreen but not of tdTomato was activated in the *ACTB–Cre* × IR1 mice (**Fig. 1e**,**f**). Similar results were obtained when the IR1 line was recombined with mouse lines that expressed recombinases that were inducible after treatment with tamoxifen[13], because of the fusion of the recombinase with an engineered domain of the estrogen hormone receptor (ER) (**Supplementary Fig. 1**). We generated mice with an inducible *CAG–Dre*^{ER} allele (**Supplementary Fig. 1a**,**b**), crossed them with the IR1 mice and evaluated expression of the reporter (**Supplementary Fig. 1c**). Tamoxifen treatment resulted in the appearance of ZsGreen^{-}tdTomato^{+} cells in tissues of *CAG-Dre*^{ER} × IR1 mice, whereas no recombination was detected in mice that had not been treated with tamoxifen (**Supplementary Fig. 1d**). Similarly, ZsGreen^{+}tdTomato^{-} cells were observed in tissues of *UBC–Cre*^{ER} × IR1 mice (UBC is broadly expressed in embryos following tamoxifen treatment) (**Supplementary Fig. 1e**,**f**). These data demonstrate that the IR1 line is responsive to both constitutive and inducible Cre and Dre recombinases.

Constitutive Dre–*rox* recombination prevents inducible Cre–*loxP* recombination

To test whether using recombination by one recombinase made the substrate unresponsive to the second recombinase, we exposed IR1 mice to constitutive Dre expression and inducible Cre^{ER} expression. We reasoned that after constitutive Dre–*rox* recombination, a cell containing the interleaved reporter sequence would no longer undergo Cre–*loxP* recombination after treatment with tamoxifen. We elected to perform these proof-of-concept experiments in cardiomyocytes. We first generated a *Tnni3–Dre* allele, in which Dre expression is driven by regulatory elements of the cardiomyocyte-specific gene troponin I3 (*Tnni3*) (**Supplementary Fig. 2a**). *Tnni3–Dre* expression specifically and efficiently labeled cardiomyocytes containing the *R26–rox–tdTomato* reporter or the interleaved reporter sequence, but not cardiomyocytes harboring the *R26–loxP–tdTomato* reporter (**Supplementary Fig. 2b–e**). We did not detect any *Tnni3–Dre* labeling of non-cardiomyocytes, such as endothelial cells, smooth muscle cells or fibroblasts (**Supplementary Fig. 2f**), demonstrating that *Tnni3–Dre* strictly targeted cardiomyocytes. To test whether Dre–*rox* recombination precluded further Cre-mediated recombination, we generated *Tnni3–Dre* × *αMHC–MerCreMer* × IR1 mice—which contain *Tnni3–Dre*, the interleaved reporter sequence and a transgene expressing a tamoxifen-inducible Cre under the control of the cardiac-specific *Myh6* gene promoter (*A1cf*$^{Tg(Myh6\text{-}cre/Esr1*)1Jmk}$; hereafter referred to as *αMHC–MerCreMer*)—and littermate control *αMHC–MerCreMer* × IR1 mice (**Supplementary Fig. 3a**). In the hearts of adult *αMHC–MerCreMer* × IR1 mice, tamoxifen induction of Cre-mediated recombination labeled 98.21 ± 0.45% of cardiomyocytes with ZsGreen (**Supplementary Fig. 3b**,**c**). However, by using the same tamoxifen induction strategy, we did not detect any ZsGreen^{+} cardiomyocytes in the hearts of *Tnni3–Dre* × *αMHC–MerCreMer* × IR1 mice, and all of the TNNI3^{+} cardiomyocytes were tdTomato^{+} (**Supplementary Fig. 3b**,**c**). These data demonstrated that constitutive Dre recombination of the interleaved reporter sequence blocked further inducible Cre–*loxP*-mediated recombination in cardiomyocytes (**Supplementary Fig. 3d**). Thus, Dre–*rox*-mediated recombination in this newly developed system could be used to preclude potential Cre–*loxP*-mediated recombination in Dre-expressing cells (for example, **Fig. 1a**, scenario 2, cell B).

Because this system relies on the dual recombinases acting on an interleaved reporter, we named it 'dual-recombinase-activated lineage tracing with interleaved reporter' (DeaLT-IR). After this experimental validation of the DeaLT-IR system for cell labeling, we next used it to address some uncertainties that have arisen from the possibility of unintentional lineage tracing in studies of putative resident stem cells in the heart and liver.

Unintentional cardiomyocyte tracing by *Kit–Cre*^{ER}

A noteworthy topic in the cardiovascular field is the myogenic fate of c-Kit^{+} cardiac stem cells (CSCs)[14–17]. In large part, this debate regarding the myogenic potential of CSCs originates from the uncertain specificity of Cre expression that is driven by regulatory elements of the *Kit* oncogene[18,19]. Indeed, we have reported that *Kit*-promoter-driven Cre expression in cardiomyocytes confounds interpretation of *Kit–Cre*^{ER} lineage tracing data[20]. The c-Kit^{+} cell population consists of two subpopulations, c-Kit^{+} cardiomyocytes and c-Kit^{+} non-cardiomyocytes; the *Kit–Cre*^{ER} allele used for lineage tracing labels both populations and does not distinguish c-Kit^{+} non-cardiomyocytes from c-Kit^{+} cardiomyocytes[20]. Therefore, we

used DeaLT-IR to prevent unintentional c-Kit$^+$ cardiomyocyte labeling by *Kit–Cre*^{ER} expression and reassessed the differentiation of c-Kit$^+$ non-cardiomyocytes to new cardiomyocytes after injury. We generated *Tnni3–Dre* × *Kit–Cre*^{ER} × IR1 mice (for the DeaLT strategy) and *Kit–Cre*^{ER} × IR1 mice (for the conventional strategy) littermates for side-by-side comparison. In the *Tnni3–Dre* × *Kit–Cre*^{ER}

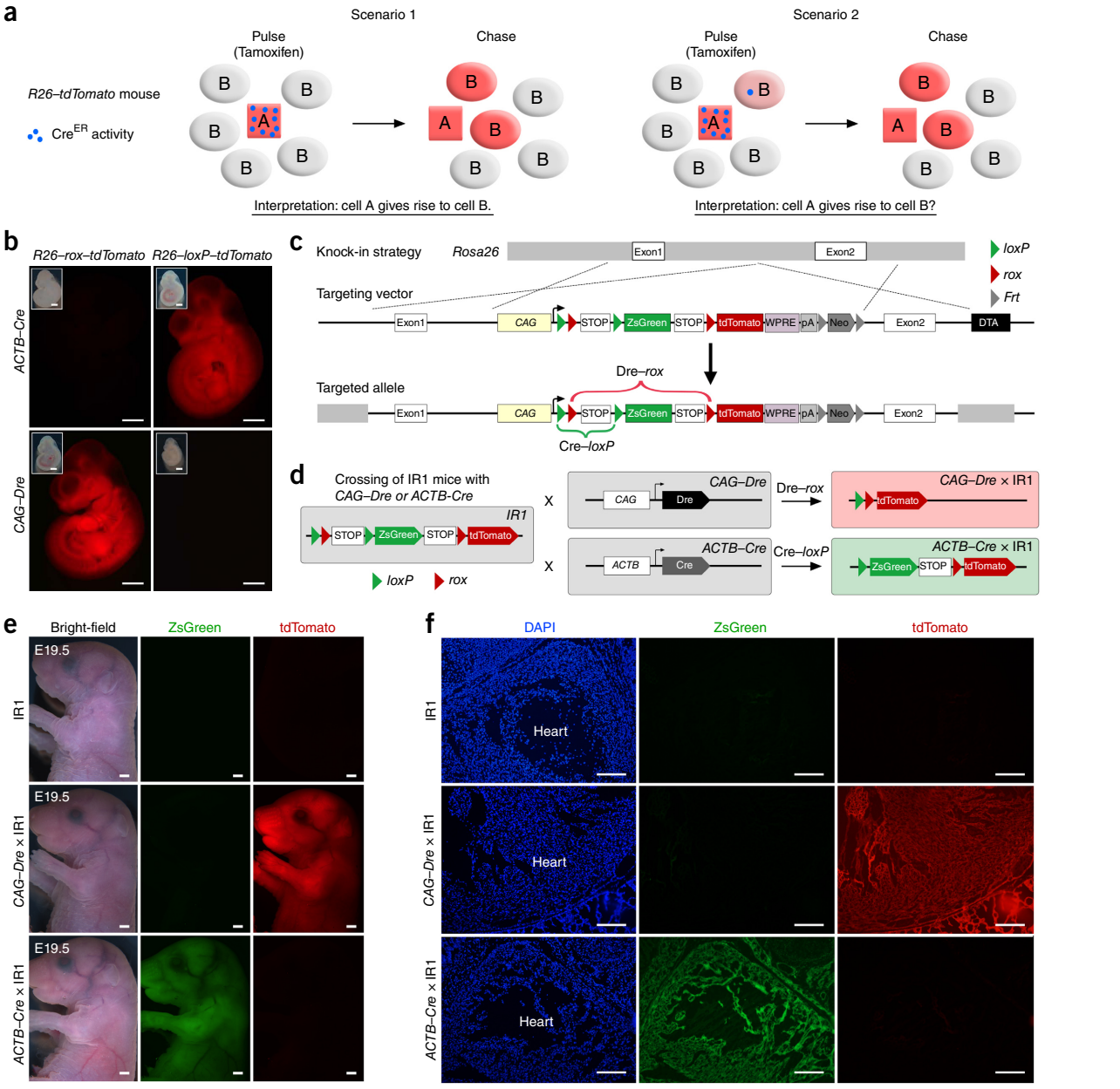

Figure 1 Generation and characterization of an interleaved reporter (IR1) mouse line. (**a**) Schematic showing how Cre activity in unintended cell types confounds lineage tracing. In cell A, which expresses Cre^{ER}, Cre–*loxP* recombination results in tdTomato expression when the mouse is treated with tamoxifen ("Pulse"). After a period of time ("Chase"), cell B is found to express tdTomato. The conclusion that cell B derives from cell A is based on the absence of Cre^{ER} expression in cell B (scenario 1). Expression of Cre^{ER} in cell B, even at trace levels, may lead to Cre–*loxP* recombination in cell B and labeling of cell B, even if cell A does not generate cell B (scenario 2). As a result, the unintended labeling of cell B in scenario 2 makes the interpretation that cell A gives rise to cell B uncertain. (**b**) Representative images showing the recombination results, as assessed by tdTomato expression, for combinations of Cre and Dre drivers (*ACTB–Cre* and *CAG–Dre*) and *rox*-flanked and *loxP*-flanked reporters (*R26–rox–tdTomato* for *R26–rox–Stop–rox–tdTomato* and *R26–loxP–tdTomato* for *R26–loxP–Stop–loxP–tdTomato*) in embryonic day 9.5 (E9.5) embryos. Scale bars, 1 mm. (**c**) Schematic showing how the IR1 reporter sequence was generated by homologous recombination. DTA, diphtheria toxin; *Neo*, neomycin resistance gene; pA, polyadenylation (polyA) sequence; *Frt*, *Frt* sequence as a substrate of the Flp recombinase; WPRE, woodchuck hepatitis virus posttranscriptional regulatory element. (**d**) Schematic showing the result of Dre–*rox* or Cre–*loxP* recombination after crossing IR1 mice with *CAG–Dre* or *ACTB–Cre* mice. (**e**) Whole-mount bright-field (left) and epifluorescence (middle and right) images showing ZsGreen (middle) and tdTomato (right) expression in IR1 (top), *CAG–Dre* × IR1 (middle) and *ACTB–Cre* × IR1 (bottom) E19.5 embryos. Scale bars, 1 mm. (**f**) Immunostained images for ZsGreen (middle) and tdTomato (right) expression in the hearts of the indicated E19.5 embryos. DAPI was used as a nuclear stain (left). The location of the heart is indicated. Scale bars, 200 μm. Each figure is representative of four individual mouse samples.

× IR1 mice, Dre first removes one *loxP* site and ZsGreen from the interleaved reporter allele in cardiomyocytes, precluding potential Cre–*loxP*-mediated labeling within cardiomyocytes. As a result, if tamoxifen activation of *Kit–Cre*^{ER} in c-Kit$^+$ non-cardiomyocytes yielded ZsGreen$^+$ cardiomyocytes after cardiac injury, then one would conclude that this was due to cardiomyocyte differentiation from c-Kit$^+$ non-cardiomyocytes rather than from the labeling of cardiomyocytes themselves (**Fig. 2a**). To achieve high labeling efficiency, we treated mice with tamoxifen 6–8 times between the neonatal and adult stages (**Fig. 2b**). In hearts from adult *Kit–Cre*^{ER} × IR1 mice, occasional ZsGreen$^+$ cardiomyocytes that were labeled by *Kit–Cre*^{ER} expression were readily observed in addition to large numbers of ZsGreen$^+$ endothelial cells (**Fig. 2c**,**d**). In contrast, we did not detect ZsGreen$^+$ cardiomyocytes in the hearts of *Tnni3–Dre* × *Kit–Cre*^{ER} × IR1 mice, whereas we observed large numbers of ZsGreen$^+$ non-myocyte cells (**Fig. 2c**,**d** and **Supplementary Fig. 4a**). Similarly, no ZsGreen$^+$tdTomato$^-$ cardiomyocytes were found after dissociating hearts from *Tnni3–Dre* × *Kit–Cre*^{ER} × IR1 mice (**Supplementary Fig. 4b**). Quantitatively, 0.74 ± 0.11% cardiomyocytes were ZsGreen$^+$tdTomato$^-$ in the hearts from *Kit–Cre*^{ER} × IR1 mice after tamoxifen treatment from the neonatal to the adult stage (**Fig. 2e**). However, not a single ZsGreen$^+$tdTomato$^-$ cardiomyocyte was detected after examination of over 500 sections from the hearts of four *Tnni3–Dre* × *Kit–Cre*^{ER} × IR1 mice, using the same tamoxifen induction strategy (**Fig. 2d**,**e**). Taken together, these results demonstrate that, in uninjured hearts, c-Kit$^+$ non-cardiomyocytes do not generate new cardiomyocytes; rather, cardiomyocytes labeled by *Kit–Cre*^{ER} expression result from Cre activity in cardiomyocytes, in which the substrate is effectively removed by the new strategy.

Although not manifest in uninjured hearts, a latent myogenic potential of c-Kit$^+$ non-cardiomyocytes might be activated by myocardial injury. To test this hypothesis, we induced myocardial infarction (MI) in *Kit–Cre*^{ER} × IR1 and *Tnni3–Dre* × *Kit-Cre*^{ER} × IR1 mice (**Fig. 2b**). The control condition was no operation (**Fig. 2c–e** and **Supplementary Fig. 4**). Four weeks after coronary artery ligation, we analyzed hearts for expression of the Cre genetic lineage tracer. We observed ZsGreen$^+$tdTomato$^-$ cardiomyocytes in the hearts of *Kit–Cre*^{ER} × IR1 mice but not in the hearts of *Tnni3–Dre* × *Kit–Cre*^{ER} × IR1 mice (**Fig. 2f**). Similarly, no ZsGreen$^+$tdTomato$^-$ cardiomyocytes were found after dissociating hearts from *Tnni3–Dre* × *Kit-Cre*^{ER} × IR1 mice (**Fig. 2g**). Whereas 0.78 ± 0.10% of cardiomyocytes were Cre-labeled (ZsGreen$^+$tdTomato$^-$) in infarcted hearts from *Kit–Cre*^{ER} × IR1 mice, no Cre-labeled cardiomyocytes (ZsGreen$^+$tdTomato$^-$) were observed in more than 500 heart sections that we examined from infarcted hearts from four *Tnni3–Dre* × *Kit–Cre*^{ER} × IR1 mice (**Fig. 2h**,**i**). We observed very few ZsGreen$^+$tdTomato$^+$ cardiomyocytes (**Fig. 2j**), consistent with fusion of c-Kit$^+$ cells with cardiomyocytes[16]. These data demonstrated that c-Kit$^+$ non-cardiomyocytes did not form *de novo* cardiomyocytes after injury (**Fig. 2k**). Unlike cardiomyocytes, endothelial cells were comparably labeled by the conventional and new strategies (**Fig. 2l**,**m**).

To independently address the myogenic potential of c-Kit$^+$ non-cardiomyocytes after cardiac injury, we generated a new Dre driver using another cardiomyocyte-specific marker, cardiac troponin T2 (*Tnnt2–Dre*) (**Supplementary Fig. 5a**). Similarly to *Tnni3–Dre*, *Tnnt2–Dre* targeted cardiomyocytes specifically and efficiently (**Supplementary Fig. 5b**,**c**). Next we generated a *Tnnt2–Dre* × *Kit–Cre*^{ER} × IR1 mouse line that permits removal of a *loxP* site in *Tnnt2–Dre*-targeted cardiomyocytes (**Supplementary Fig. 5d**). In the heart tissues from both mice that had been subjected to MI and those that had a sham surgery, we did not detect any ZsGreen$^+$tdTomato$^-$ cardiomyocytes (**Supplementary Fig. 5e–g**), whereas endothelial cells were efficiently labeled (**Supplementary Fig. 5h**,**i**). Taken together, these results indicate that c-Kit$^+$ non-cardiomyocytes do not generate new cardiomyocytes after injury.

Genetic lineage switch uncovered by new strategy

We next asked whether the DeaLT-IR strategy was sensitive enough to uncover cell lineage conversion events, by studying the known conversion of hepatocytes into new biliary epithelial cells (BECs) after liver injury[21] as a proof of concept. We first generated a mouse line bearing an inducible, hepatocyte-specific Cre using regulatory elements from the albumin gene (*Alb–Cre*^{ER}) (**Supplementary Fig. 6a**). After treatment of adult *Alb–Cre*^{ER} × IR1 mice with tamoxifen, we detected the Cre-activated reporter ZsGreen in HNF4a$^+$ hepatocytes but not in KRT19$^+$ (also known as CK19$^+$) BECs (**Supplementary Fig. 6b–d**). We next generated a *Krt19–Dre* line, which constitutively labeled BECs and also a subset of hepatocytes (**Supplementary Fig. 6e–h**). We crossed both sets of mice to produce *Krt19–Dre* × *Alb–Cre*^{ER} × IR1 mice (DeaLT-IR strategy), in which CK19$^+$ BECs expressed tdTomato and in which most HNF4a$^+$ hepatocytes were marked by ZsGreen (**Fig. 3a**). To test whether HNF4a$^+$ hepatocytes (ZsGreen$^+$) generated new CK19$^+$ BECs after injury, we exposed *Alb–Cre*^{ER} × IR1 and *Krt19–Dre* × *Alb–Cre*^{ER} × IR1 mice to the liver toxin 3,5-diethoxycarbonyl-1,4-dihydrocollidine (DDC) or to bile duct ligation (BDL) surgery[22], and we collected livers for analysis before and after injury (**Fig. 3b** and **Supplementary Fig. 7a**). After DDC-induced liver injury we found that there was substantial fibrotic tissue formation (**Fig. 3c**) and ductal reaction (**Fig. 3d**). Before DDC treatment, *Alb–Cre*^{ER} expression labeled most of the hepatocytes and did not label BECs, as no ZsGreen$^+$ BECs were evident using either the conventional or new strategy (**Fig. 3e**). After DDC-induced injury, a subset of CK19$^+$ BECs expressed ZsGreen using either strategies (**Fig. 3f**). Quantification of the percentage of ZsGreen$^+$ BECs showed that there was no difference in efficiency of hepatocyte-to-BEC conversion between the conventional and DeaLT-IR strategies (**Fig. 3g**). Similarly, we found ZsGreen$^+$ BECs in livers from mice that had been subjected to BDL surgery (**Supplementary Fig. 7b–d**), consistent with a previous study[21]. Thus, even with rigorous exclusion of the possibility of unintentional Cre labeling using the new strategy, we detected the Cre hepatic lineage tracer in BECs, which was indicative of lineage conversion of hepatocytes to BECs (**Fig. 3h**).

Generation of a nested reporter for two inducible recombinases

The DeaLT-IR strategy using the IR sequence reported above requires sequential recombination by Dre–*rox* first and then by Cre–*loxP*. However, at times it would be desirable for both Dre and Cre to be under tamoxifen control, for example, during embryonic development, albumin is expressed in hepatoblasts, which give rise to both hepatocytes and BECs[23]. Thus, the constitutive *Alb–Dre* line may target BECs in addition to hepatocytes, reducing its usefulness in distinguishing between the hepatocyte and BEC lineages. To accommodate temporally controlled Dre–*rox* recombination, we developed a second strategy in which inducible Dre–*rox* recombination controls Cre-mediated lineage tracing. This strategy uses dual recombinases with nested recombinase target sites, so that Dre–*rox* recombination removes *loxP* sites and the Cre–*loxP* readout, preventing Cre–*loxP*-mediated lineage tracing but not the reverse (**Fig. 4a**,**b**). To

implement this new strategy, we generated a mouse line expressing a new reporter allele, nested reporter 1 (NR1). Unlike the IR reporter, which requires sequential recombination, the NR1 sequence permits simultaneous expression of inducible Cre^{ER} and Dre^{ER} recombinases; however, similarly to the IR reporter, Dre–*rox* recombination controls Cre-mediated lineage tracing (**Fig. 4a**,**b**). As expected, embryos

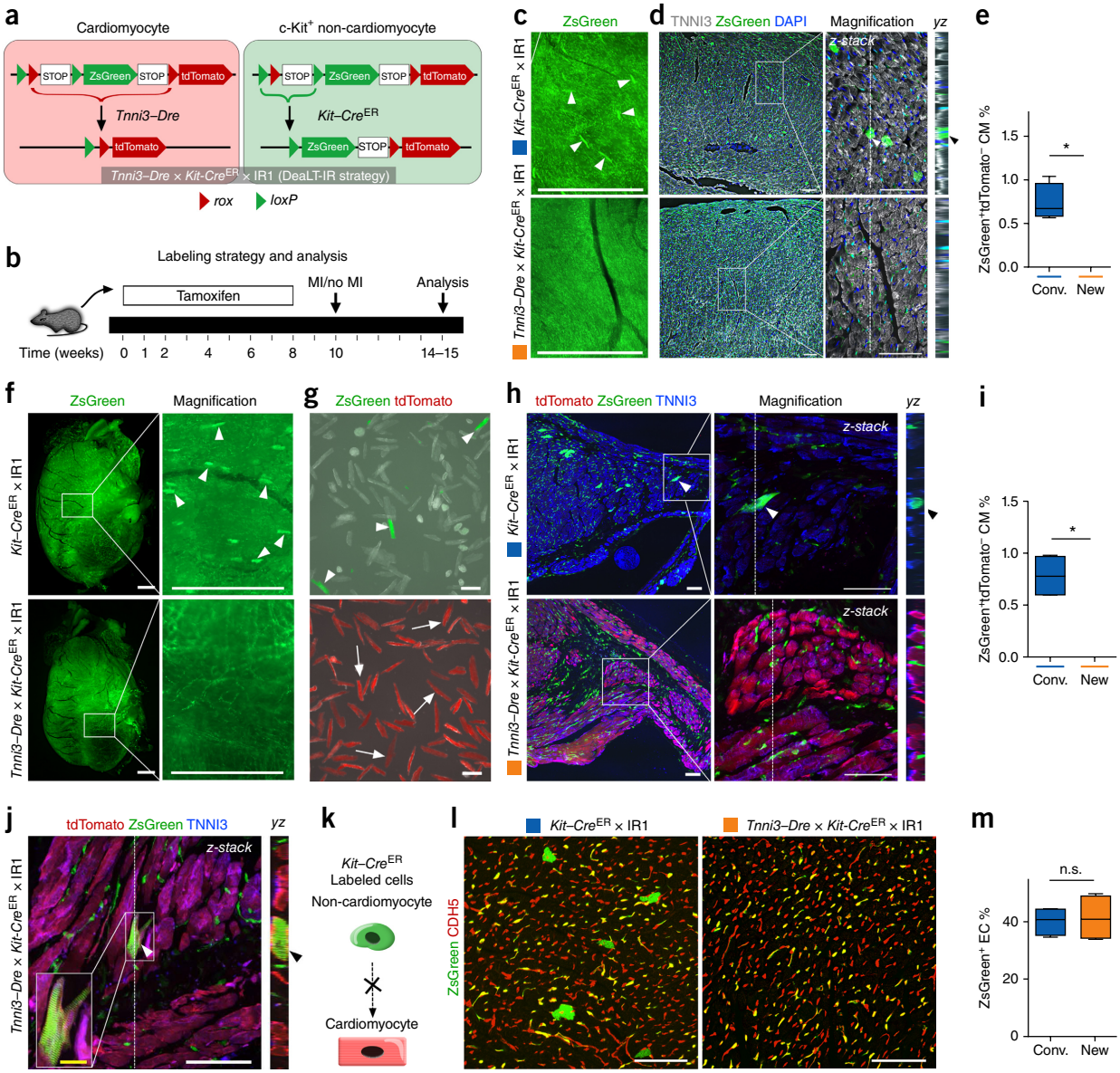

Figure 2 c-Kit+ non-cardiomyocytes do not generate cardiomyocytes. (**a**) Schematic showing the DeaLT-IR strategy for lineage tracing of c-Kit+ non-cardiomyocytes (ZsGreen+). See text for details. (**b**) Schematic showing the experimental timeline for tamoxifen treatment, operation and analysis. After tamoxifen administration, the mice were subjected to MI or no operation. (**c**,**d**) Whole-mount epifluorescence images (**c**) and images of sections showing staining for ZsGreen, TNNI3 and DAPI (**d**) in uninjured hearts from *Kit–Cre*^{ER} × IR1 and *Tnni3–Dre* × *Kit–Cre*^{ER} × IR1 mice, which represent the conventional and new lineage-tracing strategies, respectively. Magnified images of the boxed areas in **d** are also shown. *yz*, orthogonal view along the dashed line in the magnified *z*-stack images. Arrowheads indicate cardiomyocytes. (**e**) Percentages of ZsGreen+tdTomato− cardiomyocytes (CM) in the indicated groups of mice ($n = 4$ mice per group). Conv., conventional strategy; New, new strategy. Data are mean ± s.e.m. $^*P < 0.05$ by Student's *t*-test. (**f**) Whole-mount fluorescence images of infarcted hearts from *Kit–Cre*^{ER} × IR1 (top) and *Tnni3–Dre* × *Kit–Cre*^{ER} × IR1 (bottom) mice. Arrowheads indicate cardiomyocytes. (**g**) Fluorescence images of cardiomyocytes dissociated from *Kit–Cre*^{ER} × IR1 (top) and *Tnni3–Dre* × *Kit–Cre*^{ER} × IR1 hearts (bottom). Arrowheads indicate Kit–Cre^{ER}-labeled cardiomyocytes; arrows indicate *Tnni3–Dre*-labeled cardiomyocytes. (**h**) Immunostained images for tdTomato, ZsGreen and TNNI3 expression in sections from infarcted hearts from the indicated mice. Arrowheads indicate a cardiomyocyte. Magnified images of the white boxed areas are also shown. (**i**) Percentages of ZsGreen+tdTomato− cardiomyocytes in the indicated groups of mice ($n = 4$ mice per group). Data are mean ± s.e.m. $^*P < 0.05$ by Student's *t*-test. (**j**) Immunostaining for tdTomato, ZsGreen and TNNI3 expression in a section from the heart of a *Tnni3–Dre* × *Kit-Cre*^{ER} × IR1 mouse showing a tdTomato+ZsGreen+ cardiomyocyte (arrowhead), suggesting that cell fusion (inset) occurred between the c-Kit+ cell (ZsGreen+) and the cardiomyocyte (tdTomato+). (**k**) Schematic showing that c-Kit+ non-cardiomyocytes do not generate cardiomyocytes after injury. (**l**) Immunostained images for ZsGreen and CDH5 expression in sections from the hearts of the indicated mice. (**m**) Percentages of ZsGreen+ endothelial cells (EC) in the indicated groups of mice ($n = 4$ mice per group). n.s., non-significant by Student's *t*-test. Scale bars, 1 mm (**c**,**f**), 100 µm (**d**,**g**,**h**,**j**,**l**), 20 µm (**j**, inset). Each figure is representative of four individual mouse samples.

bearing the NR1 reporter did not express fluorescent protein in the absence of Cre or Dre; they expressed tdTomato but not ZsGreen in the presence of *CAG–Dre* and expressed ZsGreen but not tdTomato in the presence of *ACTB–Cre* (**Fig. 4c–e**). Having established the NR1 mouse line, we next used it to address a long-standing debate in liver regeneration.

SOX9⁺ BECs contribute to ductal cells but not hepatocytes after injury

After liver injury, the ability of SOX9⁺ BECs to give rise to new hepatocytes to regenerate the liver has been a matter of debate. Recent studies have reached contrasting conclusions, with data showing that SOX9⁺ liver progenitors contribute to hepatocytes minimally

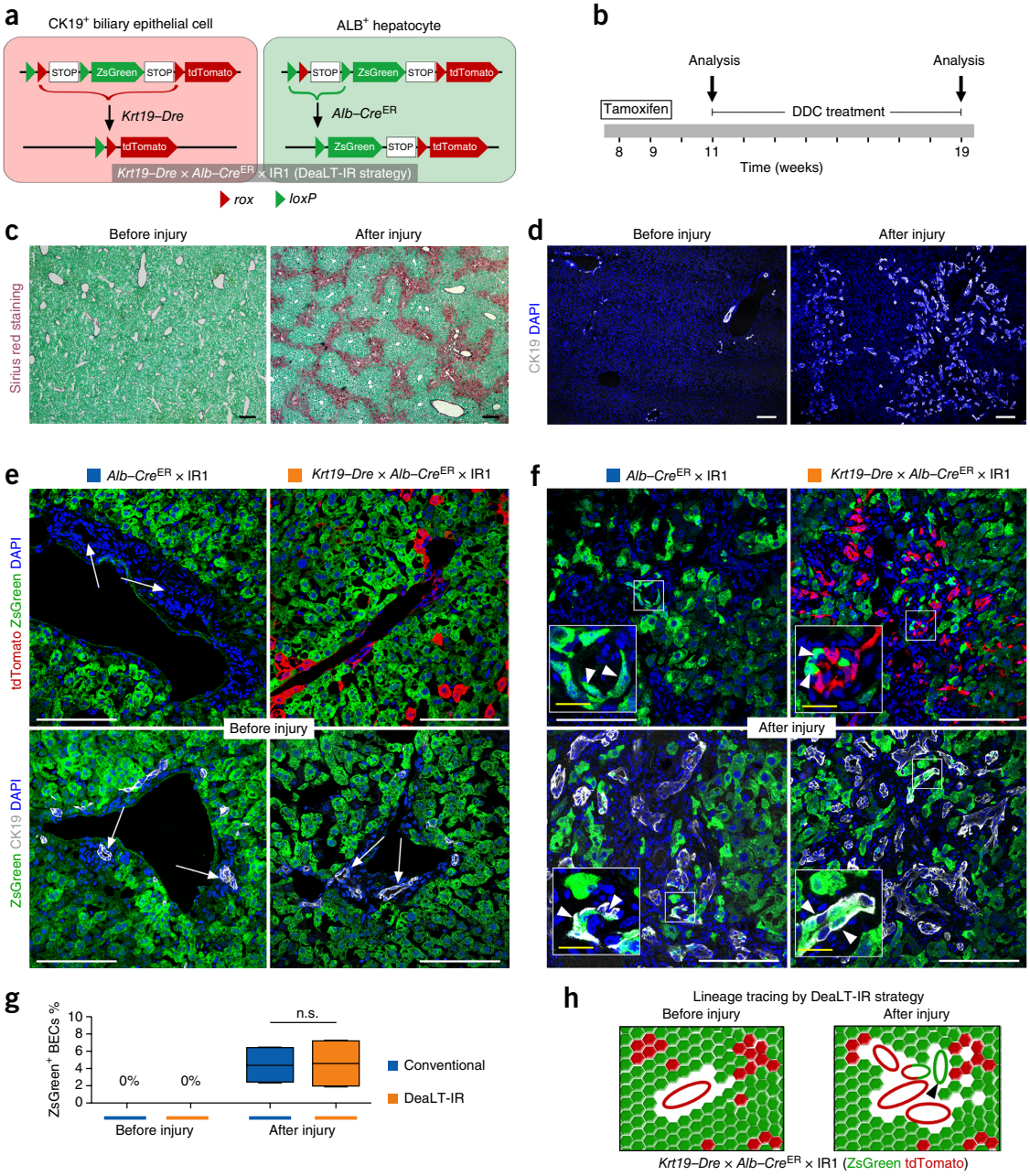

Figure 3 Hepatocyte-to-ductal cell conversion is uncovered by the DeaLT-IR strategy. (**a**) Schematic showing tdTomato labeling of CK19⁺ BECs by Dre–*rox* recombination. After tamoxifen induction, ALB⁺ hepatocytes but not BECs will be ZsGreen-labeled by Cre–*loxP* recombination. (**b**) Schematic showing the experimental timeline for cell labeling with tamoxifen, injury by DDC treatment and analysis. (**c**,**d**) Sirius red staining to assess fibrosis (**c**) and CK19 immunostaining to assess the ductal reaction (**d**) of liver sections of *Krt19–Dre* × *Alb–Cre*^{ER} × IR1 mice before (left) and after (right) injury. Nuclei were stained with DAPI. (**e**,**f**) Immunostained images for expression of ZsGreen and either tdTomato (top) or CK19 (bottom) in liver sections from *Alb–Cre*^{ER} × IR1 (conventional strategy) or *Krt19–Dre* × *Alb–Cre*^{ER} × IR1 (DeaLT-IR strategy) mice before (**e**) and after (**f**) injury. ALB–Cre^{ER} labels hepatocytes but not BECs (arrows) before injury. After injury, a few ZsGreen⁺ cells (arrowheads) exhibit ductal-cell-like morphology and express the BEC marker CK19. (**g**) Percentages of ZsGreen⁺ BECs before and after injury, as determined using each of the two strategies ($n = 4$ mice per group). Data are mean ± s.e.m. n.s., non-significant by Student's *t*-test. (**h**) Cartoon showing that a subset of new BECs (arrowhead) is derived from ZsGreen⁺ hepatocytes after injury. Scale bars, 200 μm (**c**), 100 μm (**d**–**f**), 20 μm (**f**, inset). Each figure is representative of four individual mouse samples.

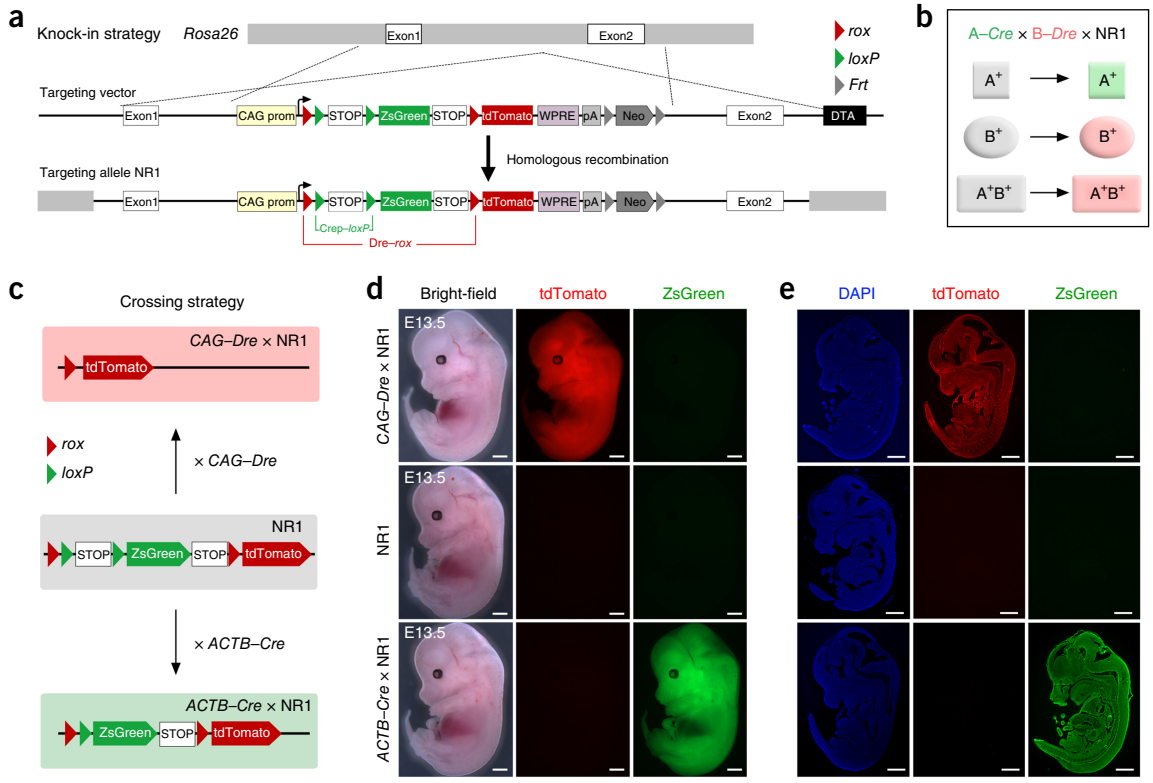

Figure 4 Generation and characterization of a secondary dual reporter system that uses nested recombinase sites. (**a**) Schematic showing the strategy for generation of the reporter in NR1 mice by homologous recombination. (**b**) Cartoon showing the pattern of cell labeling using the A–*Cre* × B–*Dre* × NR1 strategy. A^+ cells express Cre under control of the 'A' promoter; B^+ cells express Dre under control of the 'B' promoter; A^+B^+ cells express both Dre and Cre. This strategy labels A^+ cells by ZsGreen, B^+ cells by tdTomato and A^+B^+ cells by tdTomato. (**c**) Schematic showing the strategy for crossing the *CAG–Dre* or *ACTB–Cre* mouse line with the NR1 line. (**d**) Whole-mount bright-field (left) and epifluorescence (middle and right) images of E13.5 NR1, *CAG–Dre* × NR1 and *ACTB–Cre* × NR1 embryos. (**e**) Immunostained images for tdTomato and ZsGreen expression on sections of embryos as in **d**. Scale bars, 1 mm (**d**,**e**). Each figure is representative of four individual mouse samples.

or substantially after injury[24,25]. Whereas SOX9 is highly enriched in BECs, it is also weakly expressed in those hepatocytes that reside close to BECs, referred to as $SOX9^+$ periportal hepatocytes[26]. Because expression of *Sox9–Cre*^{ER} labels both BECs and a subset of periportal hepatocytes, it has been difficult to resolve whether $SOX9^+$ BECs or $SOX9^+$ hepatocytes give rise to new hepatocytes after injury. To address this question, we generated two inducible recombinase lines, *Alb–Dre*^{ER} mice and *Sox9–Cre*^{ER} mice (**Supplementary Fig. 8a**,**d**). We verified the recombination pattern in *Alb–Dre*^{ER} mice and in *Sox9–Cre*^{ER} mice using the NR1 reporter. After tamoxifen treatment, the NR1 reporter sequence was selectively recombined in the hepatocytes that expressed *Alb–Dre*^{ER}: ~99.9% $HNF4a^+$ hepatocytes and 0% $CK19^+$ BECs were $tdTomato^+ZsGreen^-$ in the liver of *Alb–Dre*^{ER} × NR1 mice (**Supplementary Fig. 8b**,**c**). This recombination pattern paralleled the *Alb–Cre*^{ER}-mediated activation of a Cre-dependent reporter (**Supplementary Fig. 6a–d**). Consistent with a previous report[26], *Sox9–Cre*^{ER} expression activated the NR1 reporter in the majority of $CK19^+$ BECs but also in a subset of $HNF4a^+$ hepatocytes (**Supplementary Fig. 8e**,**f**). Additionally, we generated a *Alb–Dre*^{ER} × *R26–rox–tdTomato* × *Sox9–Cre*^{ER} × *R26–loxP–GFP* mouse line and detected $SOX9^+ALB^+$ hepatocytes and $SOX9^+ALB^-$ BECs, along with $SOX9^-ALB^+$ hepatocytes, in the liver of these mice (**Supplementary Fig. 9**). Taken together, these data demonstrate that *Sox9–Cre*^{ER} expression labels both BECs and a subset of hepatocytes.

To test whether $SOX9^+$ BECs gave rise to new hepatocytes after injury, we generated *Alb–Dre*^{ER} × *Sox9–Cre*^{ER} × NR1 mice (DeaLT with nested reporter (DeaLT-NR) strategy), as well as *Sox9–Cre*^{ER} × NR1 littermate controls (conventional strategy) for side-by-side comparison. We performed tamoxifen treatment multiple times before liver injury and collected samples before and after the injury (**Fig. 5a**). The DeaLT-NR strategy labeled $SOX9^+$ BECs with ZsGreen, whereas $SOX9^+$ periportal hepatocytes were labeled by tdTomato owing to excision of the Cre-activated reporter ZsGreen by Dre–*rox* recombination (**Fig. 5b**,**c**). During the chase period, if chronic liver injury by treatment of the mice with carbon tetrachloride (CCl_4) induced BECs to differentiate into hepatocytes, then we would expect to observe the $ZsGreen^+tdTomato^-$ lineage mark in a subset of hepatocytes following injury but not before it. Consistent with published results[26], in pre-injury samples the conventional strategy using *Sox9–Cre*^{ER} × NR1 mice labeled both BECs and periportal hepatocytes with ZsGreen (**Fig. 5d**,**e** and **Supplementary Fig. 8f**). Quantitatively, 98.21 ± 0.85% $CK19^+$ BECs and 7.89 ± 1.31% $HNF4a^+$ periportal hepatocytes expressed ZsGreen. With the DeaLT-NR strategy, in pre-injury samples from the *Alb–Dre*^{ER} × *Sox9–Cre*^{ER} × NR1 mice, 98.82 ± 0.54% $CK19^+$ BECs were labeled by ZsGreen (**Fig. 5e**). However, no $ZsGreen^+tdTomato^-HNF4a^+$ hepatocytes were observed out of >400 liver sections from four mice, and >99.9% of the $HNF4a^+$ hepatocytes were $tdTomato^+$ (**Fig. 5e**). These results indicated that Dre–*rox* recombination occurred efficiently in hepatocytes, where it abolished unwanted Cre–*loxP* recombination (**Fig. 5b–e**). Thus, the DeaLT-NR strategy permits specific and efficient genetic labeling of $SOX9^+$ BECs with ZsGreen and $HNF4a^+$ hepatocytes with tdTomato (**Fig. 5e**).

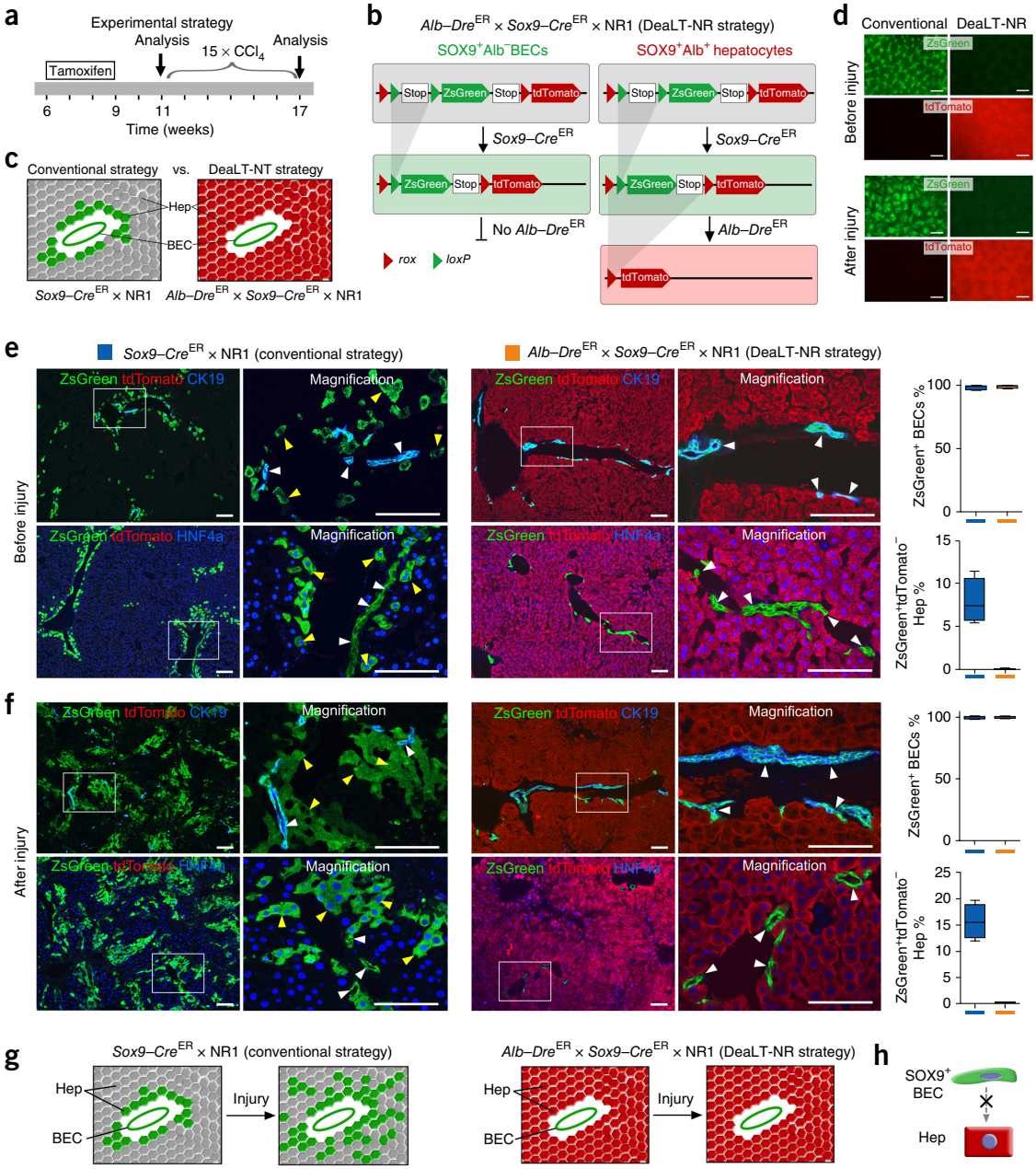

Figure 5 SOX9⁺ biliary epithelial cells adopt a ductal cell fate but not a hepatocyte fate after injury. (**a**) Schematic showing the experimental timeline for cell labeling with tamoxifen, injury with CCl_4 and analysis. (**b**) Schematic showing the patterns of Cre- and Dre-mediated recombination in BECs and hepatocytes of *Alb–Dre*^{ER} × *Sox9–Cre*^{ER} × NR1 mice. (**c**) Cartoon showing the differences in how BECs and hepatocytes (Hep) are labeled by the conventional strategy (*Sox9–Cre*^{ER} × NR1) and by the DeaLT-NR strategy (*Alb–Dre*^{ER} × *Sox9–Cre*^{ER} × NR1). (**d**) Whole-mount fluorescence images for ZsGreen and tdTomato expression in liver before and after injury, using either the conventional or DeaLT-NR strategy. (**e**,**f**) Immunostained images of liver sections for expression of ZsGreen, tdTomato, CK19 and HNF4a before (**e**) or after (**f**) injury, labeled by either the conventional (left) or DeaLT-NR (right) strategies. White arrowheads indicate BECs; yellow arrowheads indicate hepatocytes. Also shown is quantification of ZsGreen⁺ BECs or hepatocytes (Hep) ($n = 4$ mice per group). Data are mean ± s.e.m. (**g**) Cartoon showing the result of *Sox9–Cre*^{ER} fate mapping by the two strategies. (**h**) Cartoon showing that SOX9⁺ BECs do not generate new hepatocytes. Scale bars, 500 μm (**d**) and 100 μm (**e**,**f**). Each figure is representative of four individual mouse samples.

After injury, whole-mount fluorescence imaging showed that the percentage of ZsGreen⁺ cells labeled by the conventional strategy increased substantially; however, this increase was not evident using the DeaLT-NR strategy (**Fig. 5d**). Immunostaining of sections from injured livers that were labeled by the conventional strategy showed that 99.10 ± 0.53% CK19⁺ BECs and 15.71 ± 1.62% HNF4a⁺ hepatocytes expressed ZsGreen. In contrast, using the DeaLT-NR strategy, 99.31 ± 0.34% CK19⁺ BECs expressed ZsGreen, and no ZsGreen⁺tdTomato⁻ HNF4a⁺ hepatocytes were observed (**Fig. 5f**). These data indicated that after liver injury, SOX9⁺ BECs remained BECs and did not undergo lineage conversion into hepatocytes (**Fig. 5g,h**).

Resources that expand the use of the IR and NR strategies

To expand the application of the IR and NR strategies, we generated additional mouse lines harboring reporters that differed in the

relative position of the recombinase sites and the fluorescent protein readouts. For the IR strategy, in addition to the IR1 mouse line, we established the IR2, IR3 and IR4 mouse lines (**Fig. 6a**). We validated these reporters by activating them with *CAG–Dre* or *ACTB–Cre* (**Fig. 6b–g**). These mouse reporter lines provide options to best fit the experimental system being studied. For example, some Cre or Cre^{ER} lines co-express GFP or tdTomato, limiting the choice of the specific lineage-tracing readout. For the NR strategy, we generated another reporter allele (NR2) that permits Cre control of Dre recombinase (**Supplementary Fig. 10a**). Crossing the NR2 mice with the

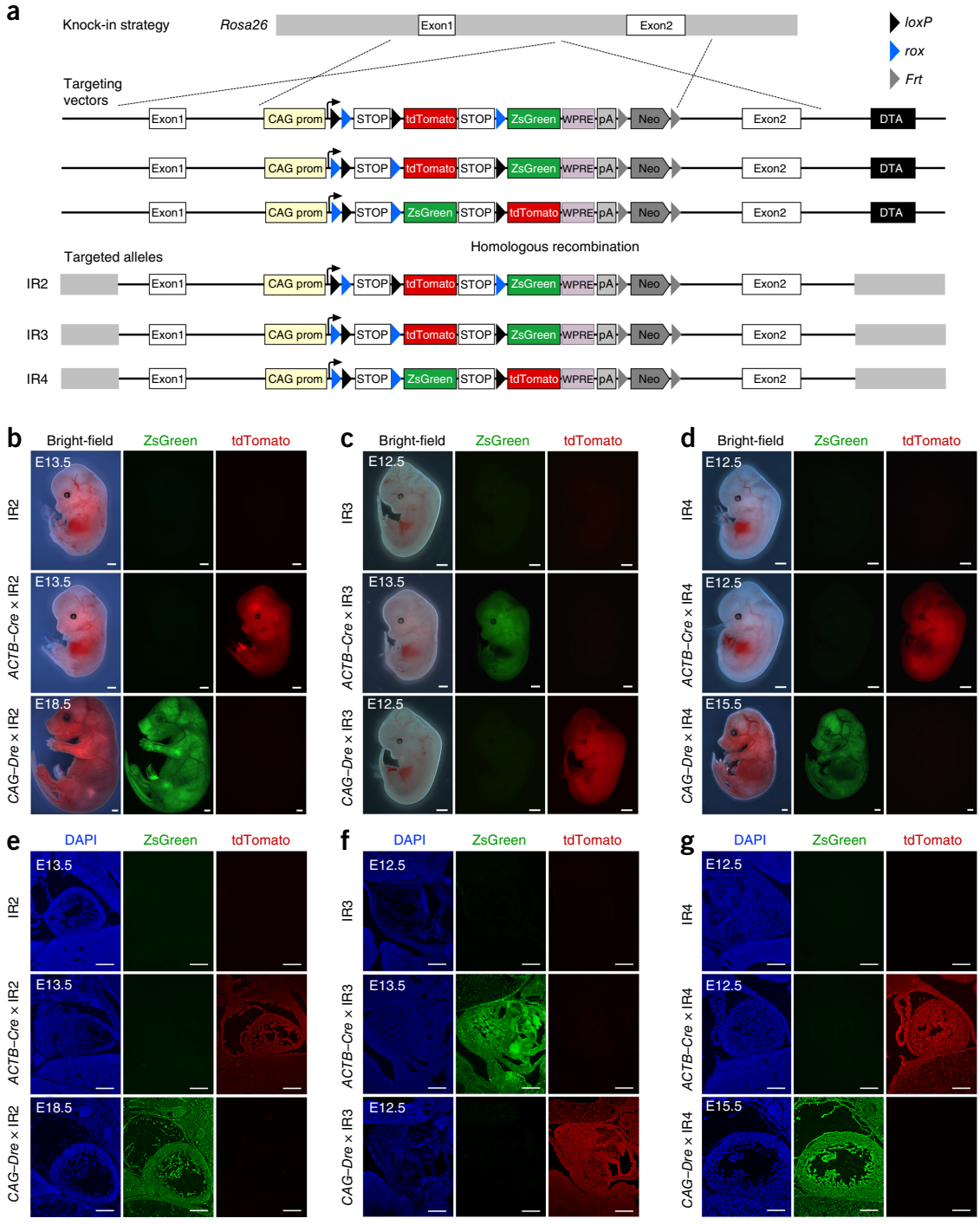

Figure 6 Generation and characterization of mice with additional interleaved reporters. (**a**) Schematic figure showing the knock-in strategy for generation of the reporter alleles in the IR2, IR3 and IR4 mice by homologous recombination. (**b–d**) Whole-mount bright-field and epifluorescence images of embryos from IR2 (**b**), IR3 (**c**) and IR4 (**d**) mice (top) and after crossing with these lines with the *ACTB–Cre* (middle) or *CAG–Dre* (bottom) lines, as indicated. Embryo ages are indicated. (**e–g**) Immunostained images for ZsGreen and tdTomato expression in sections of embryos from IR2 (**e**), IR3 (**f**) and IR4 (**g**) mice before (top) and after crossing with *ACTB–Cre* (middle) or *CAG–Dre* (bottom) mice. Scale bars, 1 mm (**b–d**) and 200 μm (**e–g**). Each image is representative of three individual embryo samples.

CAG–Dre or *ACTB–Cre* mice verified that this reporter yields the expected results (**Supplementary Fig. 10b–e**). These mouse lines provide multiple options for lineage tracing, facilitating the application of the IR and NR strategies to diverse experimental settings.

DISCUSSION

Here we developed a new tracing strategy that uses dual recombinases to resolve the uncertainty that is potentially created by recombinase expression in nontargeted cells. Using interleaved or nested reporter designs, we showed that Dre-mediated recombination effectively blocked unwanted Cre activity and Cre reporter readout, thereby clarifying the interpretation of lineage tracing data. We then applied the DeaLT-IR or DeaLT-NR strategies in proof-of-concept studies to address two debates over the plasticity of stem cells in regenerative biology. First, we addressed the debate concerning the contribution of c-Kit$^+$ CSCs to the cardiomyocyte lineage[15–17,20]. The observations that c-Kit$^+$ cells in the heart consist of both c-Kit$^+$ cardiomyocytes and c-Kit$^+$ non-cardiomyocytes and that *Kit–Cre*^{ER} is expressed in cardiomyocytes during lineage tracing[20] has complicated the interpretation of lineage tracing studies. By taking into consideration, and controlling for, *Kit–Cre*^{ER} activity in cardiomyocytes, we show that c-Kit$^+$ non-cardiomyocytes do not generate new cardiomyocytes in the postnatal heart during homeostasis and after injury. Our lineage tracing study does not directly address the question of whether c-Kit$^+$ cardiomyocytes can contribute to the formation of new cardiomyocytes after cardiac injury, but previous studies have reported that c-Kit$^+$ cells minimally contribute to cardiomyocytes after injury[16,20,27]. Our study focused on adult hearts and does not rule out the cardiomyogenic potential of c-Kit$^+$ CSCs in fetal hearts, as suggested by a recent study reporting that c-Kit$^+$ CSCs originating from neural crest possess full cardiomyogenic capacity at embryonic stages[28].

Second, we resolved the long-standing question on whether SOX9$^+$ hepatic progenitors differentiate into new hepatocytes during liver regeneration. Using conventional Cre–*loxP*-mediated lineage tracing, previous studies were unable to determine the extent to which SOX9$^+$ BEC-to-hepatocyte conversion occurs, because *Sox9–Cre*^{ER} labels both SOX9$^+$ BECs and a subset of periportal hepatocytes. By using our new strategy, we were able to label and trace SOX9$^+$ BECs distinctly and avoid tracing of pre-existing SOX9$^+$ hepatocytes. Our data support the conclusion that SOX9$^+$ BECs adopt a ductal cell but not hepatocyte fate after injury, whereas SOX9$^+$ hepatocytes expand to generate new hepatocytes, consistent with previous studies[24,29,30].

To achieve selective lineage tracing, previous studies have used an intersectional recombinase strategy. Several alleles designed for an intersectional approach have been reported, including *R26::FLAP*[31], *RC::FrePe*[28,32], *RC::Fela*[28,33] and *RC::RLTG*[34,35]. For these reporters, recombination by two different recombinases labels cells in which both recombinases are active with a distinct reporter, distinguishing them from cells labeled by only one of the recombinases. Similarly, we found that Cre and Dre drivers and their corresponding reporter alleles, when combined together in a single mouse, can distinguish single- from double-positive recombinase cells (**Supplementary Fig. 9**). Here we added a new set of reporters that enrich this rapidly evolving field for more precise lineage tracing (**Supplementary Table 1**). Among these reporters, the interleaved set is unique because it reports on the temporal sequence of recombination, unlike the intersectional and nested strategies. In comparing the intersectional and nested strategies, the intersectional strategy is optimal for identifying cells in which both recombinases are active, whereas the nested strategy is designed to identify cells in which one recombinase and not the other is active (for NR1, Cre but not Dre is active; for NR2, Dre but not Cre is active). As compared with single-recombinase-mediated tracing, the use of dual recombinases and their corresponding reporters enabled more stringent, accurate and sophisticated fate-mapping studies.

The IR or NR strategy not only provides more precise control of Cre recombinase and sets a higher technical standard for lineage tracing of Cre-expressing cells, but it also is sensitive enough to detect positive lineage-conversion events *in vivo*. By using hepatocyte-to-BEC conversion in liver injury as an example, our IR strategy was able to clearly demonstrate *in vivo* conversion of hepatocytes to BECs. Thus, this new strategy can be used to uncover cell fate switches while also rigorously controlling for potential nontargeted Cre-mediated lineage tracing.

As with any recombinase system, there are caveats to the use of these new lineage tracing strategies. Here we refer to a cell lineage as a population of cells that is labeled by a recombinase system. These population-level studies do not address the question of the types of cells that arise from individual precursor cells, which would require study of the clonal derivatives of individual precursors. However, we note that the recombinase systems described in this study could be used for clonal analyses.

The DeaLT-IR and DeaLT-NR systems require a Cre-expressing mouse line, a Dre-expressing mouse line, and the appropriate reporter line. Because we have already generated and validated several reporters, and Cre lines are often widely available, application of these new strategies will typically require generation of a Dre mouse line (**Supplementary Fig. 11a**). We propose that when a positive lineage result is detected by single-recombinase-mediated tracing, but there is uncertainty regarding the expression of Cre or the gene that drives Cre, our systems could be used for further fate mapping. A robust promoter should be selected to drive expression of Dre or Dre^{ER}, because incomplete or inefficient recombination by Dre or Dre^{ER} would not fully preclude unintentional Cre–*loxP*-mediated recombination in Dre-expressing cells. Inclusion of the woodchuck hepatitis virus posttranscriptional regulatory element (WPRE) after the *Dre* cDNA sequence could be considered for the purpose of stabilizing the Dre-encoding mRNA and increasing Dre protein levels, which might result in greater recombination efficiency. Furthermore, the specificity of the genetic elements available to express Dre in cell B is critical to the overall experimental design and to the choice of Dre or Dre^{ER}: if promoter B is specific to cell B throughout all stages of development, then the use of Dre and an interleaved reporter would be most effective, but if promoter B is specific only within a given time window, then use of Dre^{ER} and a nested reporter are recommended (**Supplementary Fig. 11a**).

In summary, by taking advantage of established and widely used Cre–*loxP*-based genetic tools, we have developed the DeaLT-IR and DeaLT-NR strategies to permit unambiguous determination of the contribution of one genetic lineage to another. These strategies are intended to reduce ambiguity in lineage tracing studies caused by uncertainty as to whether Cre is expressed in pre-existing, nontargeted cells (**Supplementary Fig. 11b**). These new strategies and reagents provide the means to more precisely dissect cell origin and fate, without invasive manipulation or cell transplantation[36–38], in multiple fields of research.

METHODS

Methods, including statements of data availability and any associated accession codes and references, are available in the online version of the paper.

Note: Any Supplementary Information and Source Data files are available in the online version of the paper.

ACKNOWLEDGMENTS

We thank B. Wu, G. Chen, Z. Weng and A. Huang for the animal husbandry and W. Bian for technical help. We thank H. Zeng at Allen Institute for sharing mouse lines and K. Anastassiadis for valuable suggestions and insightful advice on this study. We thank Shanghai Model Organisms Center, Inc. (SMOC) and Nanjing Biomedical Research Institute of Nanjing University for the generation of mouse lines. This work was supported by the Strategic Priority Research Program of the Chinese Academy of Sciences (CAS) (grant no. XDB19000000; B.Z.), the National Science Foundation of China (grant no. 31730112 (B.Z.), 91639302 (B.Z.), 31625019 (B.Z.), 31571503 (X.T.), 31501172 (H. Zhang), 31601168 (Q.L.) and 31701292 (L.H.)), the National Key Research and Development Program of China (grant no. 2017YFC1001303 (L.H.) and 2016YFC1300600 (X.T.)), the Youth Innovation Promotion Association of CAS (award no. 2015218; X.T.), the Key Project of Frontier Sciences of CAS (grant no. QYZDB-SSW-SMC003; B.Z.), the International Cooperation Fund of CAS (B.Z.), the National Program for Support of Top-notch Young Professionals (B.Z.), the Shanghai Science and Technology Commission (grant no. 17ZR1449600 (B.Z.) and 17ZR1449800 (X.T.)), the Young Elite Scientists Sponsorship Program by the China Association for Science and Technology (Q.L. and L.H.), the Shanghai Yangfan Project (award no. 15YF1414000 (H. Zhang) and 16YF1413400 (L.H.)) and Rising-Star Program (grant no.15QA1404300; X.T.), the China Postdoctoral Science Foundation (Y.W., Q.L. and J.T.), the President Fund of Shanghai Institutes for Biological Sciences (SIBS) (B.Z.), Astrazeneca (B.Z.), Sanofi-SIBS Fellowship (X.T. and L.H.), Boehringer Ingelheim (B.Z.) and a Royal Society–Newton Advanced Fellowship (B.Z.).

AUTHOR CONTRIBUTIONS

L.H. and B.Z. designed the study, performed experiments and analyzed the data; Yan Li, Yi Li, W.P., X.H., X.T., Y.W., H. Zhang, Q.L., L.Z., H. Zhao and J.T. bred the mice and performed experiments; D.C., H.J., Zhibo Han, Zhongchao Han, Y.N., S.H., Q.-D.W., R.S., J.F., Y.Y. and H.H. analyzed data, provided technical support and edited the manuscript; F.W. and T.C. provided mouse lines; W.T.P. provided intellectual input and edited the manuscript; B.Z. conceived and supervised the study, analyzed the data and wrote the manuscript.

COMPETING FINANCIAL INTERESTS

The authors declare no competing financial interests.

1. Laugwitz, K.L. *et al.* Postnatal Isl1$^+$ cardioblasts enter fully differentiated cardiomyocyte lineages. *Nature* **433**, 647–653 (2005).
2. Smart, N. *et al. De novo* cardiomyocytes from within the activated adult heart after injury. *Nature* **474**, 640–644 (2011).
3. Chen, Q. *et al.* Endothelial cells are progenitors of cardiac pericytes and vascular smooth muscle cells. *Nat. Commun.* **7**, 12422 (2016).
4. Kumar, M.E. *et al.* Defining a mesenchymal progenitor niche at single-cell resolution. *Science* **346**, 1258810 (2014).
5. Snippert, H.J. *et al.* Intestinal crypt homeostasis results from neutral competition between symmetrically dividing Lgr5 stem cells. *Cell* **143**, 134–144 (2010).
6. Klotz, L. *et al.* Cardiac lymphatics are heterogeneous in origin and respond to injury. *Nature* **522**, 62–67 (2015).
7. Sauer, B. & Henderson, N. Site-specific DNA recombination in mammalian cells by the Cre recombinase of bacteriophage P1. *Proc. Natl. Acad. Sci. USA* **85**, 5166–5170 (1988).
8. Nagy, A. Cre recombinase: the universal reagent for genome tailoring. *Genesis* **26**, 99–109 (2000).
9. Davis, J., Maillet, M., Miano, J.M. & Molkentin, J.D. Lost in transgenesis: a user's guide for genetically manipulating the mouse in cardiac research. *Circ. Res.* **111**, 761–777 (2012).
10. Tian, X., Pu, W.T. & Zhou, B. Cellular origin and developmental program of coronary angiogenesis. *Circ. Res.* **116**, 515–530 (2015).
11. Sauer, B. & McDermott, J. DNA recombination with a heterospecific Cre homolog identified from comparison of the *pac-c1* regions of P1-related phages. *Nucleic Acids Res.* **32**, 6086–6095 (2004).
12. Anastassiadis, K. *et al.* Dre recombinase, like Cre, is a highly efficient site-specific recombinase in *E. coli*, mammalian cells and mice. *Dis. Model. Mech.* **2**, 508–515 (2009).
13. Guo, C., Yang, W. & Lobe, C.G. A Cre recombinase transgene with mosaic, widespread tamoxifen-inducible action. *Genesis* **32**, 8–18 (2002).
14. Beltrami, A.P. *et al.* Adult cardiac stem cells are multipotent and support myocardial regeneration. *Cell* **114**, 763–776 (2003).
15. Ellison, G.M. *et al.* Adult c-Kit$^+$ cardiac stem cells are necessary and sufficient for functional cardiac regeneration and repair. *Cell* **154**, 827–842 (2013).
16. van Berlo, J.H. *et al.* c-Kit$^+$ cells minimally contribute cardiomyocytes to the heart. *Nature* **509**, 337–341 (2014).
17. Hatzistergos, K.E. *et al.* Stimulatory effects of MSCs on c-Kit$^+$ cardiac stem cells are mediated by SDF1–CXCR4 and SCF–c-Kit signaling pathways. *Circ. Res.* **119**, 921–930 (2016).
18. Molkentin, J.D. & Houser, S.R. Are resident c-Kit$^+$ cardiac stem cells really all that are needed to mend a broken heart? *Circ. Res.* **113**, 1037–1039 (2013).
19. Molkentin, J.D. Letter by Molkentin regarding article, "The absence of evidence is not evidence of absence: the pitfalls of *Cre* knock-ins in the c-Kit locus". *Circ. Res.* **115**, e21–e23 (2014).
20. Liu, Q. *et al.* Genetic lineage tracing identifies *in situ* Kit-expressing cardiomyocytes. *Cell Res.* **26**, 119–130 (2016).
21. Yanger, K. *et al.* Robust cellular reprograming occurs spontaneously during liver regeneration. *Genes Dev.* **27**, 719–724 (2013).
22. Pu, W. *et al.* Mfsd2a$^+$ hepatocytes repopulate the liver during injury and regeneration. *Nat. Commun.* **7**, 13369 (2016).
23. Zorn, A.M. & Wells, J.M. Vertebrate endoderm development and organ formation. *Annu. Rev. Cell Dev. Biol.* **25**, 221–251 (2009).
24. Tarlow, B.D., Finegold, M.J. & Grompe, M. Clonal tracing of Sox9$^+$ liver progenitors in mouse oval cell injury. *Hepatology* **60**, 278–289 (2014).
25. Furuyama, K. *et al.* Continuous cell supply from a Sox9-expressing progenitor zone in adult liver, exocrine pancreas and intestine. *Nat. Genet.* **43**, 34–41 (2011).
26. Font-Burgada, J. *et al.* Hybrid periportal hepatocytes regenerate the injured liver without giving rise to cancer. *Cell* **162**, 766–779 (2015).
27. Sultana, N. *et al.* Resident c-Kit$^+$ cells in the heart are not cardiac stem cells. *Nat. Commun.* **6**, 8701 (2015).
28. Hatzistergos, K.E. *et al.* c-Kit$^+$ cardiac progenitors of neural crest origin. *Proc. Natl. Acad. Sci. USA* **112**, 13051–13056 (2015).
29. Carpentier, R. *et al.* Embryonic ductal plate cells give rise to cholangiocytes, periportal hepatocytes and adult liver progenitor cells. *Gastroenterology* **141**, 1432–1438 (2011).
30. Yanger, K. *et al.* Adult hepatocytes are generated by self-duplication rather than stem cell differentiation. *Cell Stem Cell* **15**, 340–349 (2014).
31. Awatramani, R., Soriano, P., Rodriguez, C., Mai, J.J. & Dymecki, S.M. Cryptic boundaries in roof plate and choroid plexus identified by intersectional gene activation. *Nat. Genet.* **35**, 70–75 (2003).
32. Engleka, K.A. *et al.* Islet1 derivatives in the heart are of both neural crest and second heart field origin. *Circ. Res.* **110**, 922–926 (2012).
33. Jensen, P. *et al.* Redefining the serotonergic system by genetic lineage. *Nat. Neurosci.* **11**, 417–419 (2008).
34. Plummer, N.W. *et al.* Expanding the power of recombinase-based labeling to uncover cellular diversity. *Development* **142**, 4385–4393 (2015).
35. Plummer, N.W., de Marchena, J. & Jensen, P. A knock-in allele of *En1* expressing Dre recombinase. *Genesis* **54**, 447–454 (2016).
36. Wang, X. *et al.* Cell fusion is the principal source of bone-marrow-derived hepatocytes. *Nature* **422**, 897–901 (2003).
37. Alvarez-Dolado, M. *et al.* Fusion of bone-marrow-derived cells with Purkinje neurons, cardiomyocytes and hepatocytes. *Nature* **425**, 968–973 (2003).
38. Vassilopoulos, G., Wang, P.R. & Russell, D.W. Transplanted bone marrow regenerates liver by cell fusion. *Nature* **422**, 901–904 (2003).

ONLINE METHODS

Detailed information on experimental design and reagents can be found in the **Life Sciences Reporting Summary**.

Mice. All mouse studies were carried out in strict accordance with the guidelines of the Institutional Animal Care and Use Committee (IACUC) at the Institute for Nutritional Sciences, Shanghai Institutes for Biological Sciences, Chinese Academy of Sciences. The *CAG–Dre*, *ACTB–Cre*, *UBC–Cre*^{ER}, *αMHC–MerCreMer*, *Kit–Cre*^{ER}, *R26–loxP–tdTomato*, *R26–rox–tdTomato* and *R26–GFP* mouse lines have been reported previously[12,20,39–43]. The interleaved reporter 1 (IR1) knock-in mouse line was generated by knocking *CAG–loxP–rox*–Stop–*loxP–ZsGreen*–polyA–*rox–tdTomato*–polyA–*Frt–Neo–Frt* into the *Rosa26* locus, as previously described[44]. Two homologous arms on the 5′ and 3′ sides of intron 1 of *Rosa26* were generated in the targeting vectors by recombination; the targeting vector was then linearized and electroporated into mouse embryonic stem (ES) cells. After G418 selection, approximately 200 clones were selected for retrieval of genomic DNA and for screening of positive clones. Neomycin-resistant clones were tested for correct gene targeting by long PCR assays with primer pairs spanning the targeting vector and flanking genomic DNA. Following verification of correct targeting and karyotype, at least two positive ES clones were expanded and injected into blastocysts for mouse generation. The obtained chimeric mouse lines were crossed to C57BL/6J lines for germline transmission. PCR primers spanning the genomic DNA and inserted cassette were designed to test for the correct genotype. Chimeric mice that were positive for the targeted ES cells were germline-transferred to the F1 generation and bred on a C57BL/6J × ICR background. Similarly, we generated the IR2 mouse line by knocking the CAG–*loxP–rox*–Stop–*loxP–tdTomato*–Stop–*rox–ZsGreen*–polyA–*Frt–Neo–Frt* cassette into the *Rosa26* locus, the IR3 mouse line by knocking the *CAG–rox–loxP*–Stop–*rox–tdTomato*–Stop–*loxP–ZsGreen*–polyA–*Frt-Neo–Frt* cassette into the *Rosa26* locus, the IR4 mouse line by knocking the *CAG–rox–loxP*–Stop–*rox–ZsGreen*–polyA–*loxP–tdTomato*–Stop–*Frt–Neo–Frt* cassette into the *Rosa26* locus, the NR1 mouse line by knocking the *Rosa26–CAG–rox–loxP*–Stop–*loxP–ZsGreen*–Stop–*rox–tdTomato*–polyA–*Frt–Neo–Frt* cassette into the *Rosa26* locus and the NR2 mouse line by knocking the *Rosa26–CAG–loxP–rox*–Stop–*rox–ZsGreen*–Stop–*loxP–tdTomato*–polyA–*Frt–Neo–Frt* cassette into the *Rosa26* locus. For these 'Stop' sequences, the first Stop sequence is triple SV40 polyA sequences, and the second Stop sequence is adapted from the polyA sequence between mT (membrane-targeted tdTomato) and mG (membrane-targeted eGFP) of pCA-mTmG (Addgene #26123). The *Alb–Cre*^{ER} knock-in mouse line was generated by knocking the cDNA sequence encoding the Cre recombinase and estrogen receptor fusion protein into the site encoding the translational start codon in the *Alb* gene. Briefly, a 129 mouse bacterial artificial chromosome (BAC) clone containing the complete mouse *Alb* gene was obtained from the Sanger Institute (UK). A targeting vector was constructed containing the following cassettes: *Cre*^{ERT2} cDNA, SV40 polyA sequence and *Frt*-flanked PGK-EM7-Neo resistance gene. Two homologous arms on the 5′ and 3′ sides of first coding exon of the *Alb* gene were generated in targeting vectors by recombination from the BAC. The targeting vector was digested with I-CeuI for linearization and then electroporated into mouse ES cells. The targeting vector containing the previously mentioned cassettes was knocked into the *Alb* locus for endogenous expression of *Cre*^{ERT2} cDNA. After G418 selection, approximately 200 clones were selected for retrieval of genomic DNA and for screening of positive clones. Neomycin-resistant clones were tested for correct gene targeting by long PCR assays with primer pairs spanning the targeting vector and flanking genomic DNA. Following verification of correct targeting and karyotype, at least two positive ES clones were expanded and injected into blastocysts for mouse generation. The resulting chimeric mouse lines were then crossed to C57BL/6J lines for germline transmission. PCR was performed to test the correct genotype, and the established *Alb–Cre*^{ER} mouse lines were maintained on a C57BL/6J × ICR background. The *Tnni3–Dre*, *Tnnt2–Dre*, *Krt19–Dre*, *Sox9–Cre*^{ER}, *Alb–Dre*^{ER} and *CAG–Dre*^{ER} knock-in mouse lines were generated by genome editing using CRISPR–Cas9 technology, as previously described[45]. A cDNA encoding the Dre recombinase was inserted into the site encoding the translational start codon of the *Tnni3* or *Krt19* gene; a cDNA encoding the Cre^{ERT2} recombinase was inserted after the site encoding the translational stop codon of the *Sox9* gene; a cDNA encoding the Dre^{ERT2} recombinase was inserted after the sequence encoding the translational stop codon of the *Alb* gene; a cDNA encoding the Dre^{ERT2} recombinase was inserted into the *Rosa26* locus. To strengthen the stability of the transcripts, we included the woodchuck hepatitis virus posttranscriptional regulatory element (WPRE) before the polyA signal sequence. The IR1, IR2, NR1, NR2, *CAG–Dre*^{ER}, *Tnni3–Dre*, *Tnnt2–Dre*, *Alb–Cre*^{ER}, *Krt19–Dre* and *Alb–Dre*^{ER} mouse lines were generated by Shanghai Model Organisms Center, Inc. (SMOC). The IR3 and IR4 mouse lines were generated by the Nanjing Biomedical Research Institution of Nanjing University, Nanjing, China. The *Sox9–Cre*^{ER} line was generated by the National Institute for Biological Sciences, Beijing, China. For induction of Cre^{ER}–*loxP* or Dre^{ER}–*rox* recombination, tamoxifen (Sigma, T5648) was dissolved in corn oil (20 mg/ml) and administered by gavage at the indicated time points (0.10–0.15 mg tamoxifen per g mouse body weight) as described previously[46]. Both male and female mice were used and were randomized into different treatment groups in all experiments.

Genomic PCR. Genomic DNA was prepared from the embryonic yolk sac or the tails of mice. Tissues were lysed by incubation with lysis buffer (100 mM Tris HCl (pH 7.8), 5 mM EDTA, 0.2% SDS, 200 mM NaCl and 100 μg/ml proteinase K) overnight at 55 °C, followed by centrifugation at maximum speed (21,130*g*) for 5 min to obtain supernatants with genomic DNA. DNA was precipitated by isopropanol, washed in 70% ethanol and dissolved in deionized water. All of the embryos and mice were genotyped using genomic PCR as described previously[47].

Whole-mount fluorescence microscopy. Mouse hearts or embryos were washed in phosphate-buffered saline (PBS) and fixed in 4% paraformaldehyde (PFA) at 4 °C for 20 min to 1 h (depending on tissue size) followed by three washes with PBS. Tissues were placed on an agar gel for whole-mount bright-field or fluorescence imaging using a Zeiss stereo microscope (AxioZoom V16).

Immunostaining. Immunostaining was performed as previously described[48]. Briefly, embryos or hearts were collected in PBS on ice and then fixed in 4% PFA at 4 °C for 20 min to 1 h depending on tissue size. After three washes in PBS, the tissues were dehydrated in a 30% sucrose in PBS solution overnight at 4 °C, then embedded in optimum cutting tissue (O.C.T., Sakura) and stored at −80 °C until sectioning. 10-μm-thick cryosections were collected on positively charged slides and stored at −20 °C until use. For immunostaining, tissue sections were blocked with PBSST (0.1% Triton X-100 and 2.5% normal donkey serum in PBS) for 30 min at room temperature, followed by incubation with the primary antibody overnight at 4 °C. The next day, tissue sections were washed three times with PBS, incubated with Alexa-Fluor-conjugated secondary antibodies (Invitrogen) for 30 min at room temperature, washed three times with PBS and mounted with mounting medium containing the nuclear stain DAPI (Vector Lab). For weak signals, we used horseradish peroxidase (HRP)- or biotin-conjugated secondary antibodies and a tyramide signal amplification kit (PerkinElmer). Antibodies to the following proteins were used: tdTomato (Rockland, 600-401-379; 1:1,000 dilution), TNNI3 (Abcam, ab56357; 1:100 dilution), CDH5 (R&D, AF1002; 1:100 dilution), PECAM (BD Pharmingen, 553370; 1:500 dilution), αSMA (Sigma, F3777; 1:500 dilution), PDGFRa (eBioscience, 14-1401-81; 1:500 dilution), CK19 (DSHB, TROMA-III; 1:500 dilution), HNF4a (Santa Cruz, sc-6556; 1:100 dilution) and GFP (Abcam, ab6662; 1:100 dilution). A polyclonal antibody to ZsGreen was obtained from immunized rabbits and characterized by immunostaining on ZsGreen^{+} tissue samples. Images from immunostained samples were acquired by using an Olympus confocal microscope (FV1200), a Leica confocal microscope (TCS SP5) or a Zeiss stereo microscope (AxioZoom V16). To obtain *z*-stack images, 5–10 consecutive *xy* images were scanned on the *z*-axis using an Olympus confocal microscope. The obtained images were analyzed by ImageJ (NIH) software. The images were merged using the Image color-merge channels function, and the *z*-stack images were obtained using the *z*-stack function in ImageJ with average intensity projection of each image taken serially in the *z*-axis. In the stack, an orthogonal view was used to reveal the signals on the *xz* or *yz* axes. Merged signals and split channels were used to delineate the signals at single-cell resolution, as described previously[41].

Quantification of labeled cardiomyocytes and endothelial cells. Mouse hearts were collected and embedded for serial coronal sectioning. For each adult heart, all of the collected sections were put on 52 to 65 positively charged slides, with six slides to a set, and each slide contained 8–10 heart sections. Slides were stained for TNNI3 and ZsGreen. The percentage of labeled cardiomyocytes was calculated as the number of $ZsGreen^{+}TNNI3^{+}$ cardiomyocytes divided by the number of $TNNI3^{+}$ cardiomyocytes. A researcher who was blinded to the groups quantified the percentage using an Olympus fluorescence microscope (BX53). Labeling of endothelial cells was quantified as the percentage of $ZsGreen^{+}CDH5^{+}$ endothelial cells in $CDH5^{+}$ endothelial cells. At least four hearts per group were quantified.

Myocardial infarction in adult mice. Adult mice (9–12 weeks of age) were subjected to surgical manipulation as described previously[49]. Briefly, mice on a heated pad were anesthetized with 2% isoflurane gas through tracheal intubation. When the mouse did not respond to a tail and toe pinch, its limbs were fixed on the pad, and its chest was disinfected with iodine. A vertical 1-cm incision was made at the chest skin, and a blunt dissection of the muscle and fascia was performed to avoid injuring the blood vessels. After making a 1-cm incision between the third and fourth intercostal ribs, the internal chest was exposed for subsequent operation. Then the left anterior descending (LAD) branch of the coronary artery was permanently ligated with a 0-8 suture. The ligation was judged to be successful when the heart showed signs of cyanosis. The incision was closed with a 6-0 suture, and air was discharged from the chest. The surgical incision was disinfected, and the mice were supplied with pure oxygen for 4–5 min until they resumed spontaneous breathing. Then the tracheal intubation tube was removed, and the mice were kept warm until recovery of normal behavior followed by treatment with analgesics. In the sham-operated control group, the same procedure was followed, except that the ligation of the LAD coronary artery was omitted. The person who performed the surgery was blinded to the allocation of the different experimental groups.

Cardiomyocyte isolation. Adult cardiomyocytes were isolated as described previously[20]. Briefly, adult mice were injected with 200 µl heparin (6.25 U/µl) intraperitoneally to prevent coagulation of blood in the coronary arteries. Twenty minutes later, the mice were anesthetized with sodium pentobarbital (80 mg per kg body weight) by intraperitoneal injection, followed by an interval of 5–10 min until the mice stopped responding to tail and toe pinches. Then the hearts were dissected and ligated to a perfusion-fluid-filled aortic cannula, and these were then perfused with perfusion buffer (137 mM NaCl, 4 mM KCl, 0.33 mM NaH_2PO_4, 1 mM $MgCl_2$, 10 mM HEPES, 5 mM taurine, 10 mM 2,3-butanedione monoxime (BDM; B0753, Sigma)) and 10 mM glucose, pH 7.4) at a flow rate of 4 ml/min for ~5 min, until the effluent became clear. The perfusion liquid was switched to digestion buffer (perfusion buffer containing 0.1 mg/µl collagenase II and 0.08 mg/µl protease XIV) and perfused for 12–15 min at the same flow rate. The digested hearts were transferred to transfer buffer (perfusion buffer containing 0.5 mg/ml BSA), minced by forceps and filtered through a 100-µm strainer. The isolated cells were centrifuged for 3 min at 20*g* to pellet the cardiomyocytes, which were subsequently resuspended in transfer buffer for further analysis.

Models of liver injury. Mice that were treated with 5-diethoxycarbonyl-1,4-dihydrocollidine (DDC), carbon tetrachloride (CCl_4) or bile duct ligation (BDL) were used as models of liver injury. All of the treatments in to cause liver injury were performed at 2 weeks after tamoxifen treatment. For the DDC model of chronic liver injury, adult mice (11 weeks of age) were given 0.1% wt/wt DDC (Sigma-Aldrich) in PMI Mouse Diet (#5015, Harlan Teklad) for 8 weeks; control mice were fed with PMI Mouse diet. For the CCl_4 model of chronic liver injury, CCl_4 was dissolved in corn oil (1:3) first, and then the mice (11 weeks of age) were given CCl_4 (1 µl per g body weight) by intraperitoneal injection once every 3 d for a total of 15 injections. Control mice received the equivalent amount of corn oil. The BDL model of liver injury was performed according to established protocols[50]. Adult mice (11 weeks of age) were anesthetized with 2% isoflurane gas in a sealed chamber. The abdominal fur was then removed, and the skin was disinfected with iodine. The mice were transferred onto a 37 °C heating pad, and anesthesia was maintained by inhalation of isoflurane. A midline abdominal incision was made to expose the liver. The common bile duct was ligated twice with 4-0 silk sutures. After the ligation, the skin incisions were closed with a 6-0 suture, and the mice were supplied with pure oxygen for 4–5 min until they resumed normal breathing. Then the tracheal intubation tube was removed, and the mice were kept warm until recovery of normal behavior. In the sham-operated group, the same procedure was followed, except that the common bile duct was not ligated.

Statistical analysis. All data were determined from three or four independent experiments as indicated in each figure legend and are presented as mean values ± s.e.m. All mice were randomly assigned to different experimental groups. Statistical comparisons between data sets were made with analysis of normality and variance. A two-sided unpaired Student's *t*-test was used for comparing differences between two groups. The null hypothesis was rejected for $P < 0.05$.

39. Ruzankina, Y. *et al.* Deletion of the developmentally essential gene *Atr* in adult mice leads to age-related phenotypes and stem cell loss. *Cell Stem Cell* **1**, 113–126 (2007).
40. Sohal, D.S. *et al.* Temporally regulated and tissue-specific gene manipulations in the adult and embryonic heart using a tamoxifen-inducible Cre protein. *Circ. Res.* **89**, 20–25 (2001).
41. Liu, Q. *et al.* c-Kit^{+} cells adopt vascular endothelial but not epithelial cell fates during lung maintenance and repair. *Nat. Med.* **21**, 866–868 (2015).
42. Madisen, L. *et al.* A robust and high-throughput Cre reporting and characterization system for the whole mouse brain. *Nat. Neurosci.* **13**, 133–140 (2010).
43. Zhang, H. *et al.* Endocardium contributes to cardiac fat. *Circ. Res.* **118**, 254–265 (2016).
44. Zhang, H. *et al.* Endocardium minimally contributes to coronary endothelium in the embryonic ventricular free walls. *Circ. Res.* **118**, 1880–1893 (2016).
45. Zhang, H. *et al.* Genetic lineage tracing identifies endocardial origin of liver vasculature. *Nat. Genet.* **48**, 537–543 (2016).
46. Liu, Q. *et al.* Genetic targeting of sprouting angiogenesis using Apln–Cre^{ER}. *Nat. Commun.* **6**, 6020 (2015).
47. Tian, X. *et al.* Sub-epicardial endothelial cells invade the embryonic ventricle wall to form coronary arteries. *Cell Res.* **23**, 1075–1090 (2013).
48. He, L. *et al.* Genetic lineage tracing discloses arteriogenesis as the main mechanism for collateral growth in the mouse heart. *Cardiovasc. Res.* **109**, 419–430 (2016).
49. Zhou, B. *et al.* Adult mouse epicardium modulates myocardial injury by secreting paracrine factors. *J. Clin. Invest.* **121**, 1894–1904 (2011).
50. Tag, C.G. *et al.* Bile duct ligation in mice: induction of inflammatory liver injury and fibrosis by obstructive cholestasis. *JoVE* **96**, e52438 (2015).

doi:10.1038/nm.4437

nature research

Corresponding author(s): Bin Zhou

☐ Initial submission ☐ Revised version ☒ Final submission

Life Sciences Reporting Summary

Nature Research wishes to improve the reproducibility of the work that we publish. This form is intended for publication with all accepted life science papers and provides structure for consistency and transparency in reporting. Every life science submission will use this form; some list items might not apply to an individual manuscript, but all fields must be completed for clarity.

For further information on the points included in this form, see Reporting Life Sciences Research. For further information on Nature Research policies, including our data availability policy, see Authors & Referees and the Editorial Policy Checklist.

Experimental design

1. Sample size

   Describe how sample size was determined.

   For all experiments, 3-4 samples were used for each condition/genotype according to standard scientific conventions, as indicated in each figure.
   For details, n=4, Figure 1-5, Supplementary Figure 1-9; n=3, Figure 6, Supplementary Figure 10.

2. Data exclusions

   Describe any data exclusions.

   All mice were included in the immunostaining analysis for study of lineage tracing, expression map or phenotype analysis.

3. Replication

   Describe whether the experimental findings were reliably reproduced.

   All replication attempts were successful.

4. Randomization

   Describe how samples/organisms/participants were allocated into experimental groups.

   For induction of CreER-loxP or DreER-rox recombinations, tamoxifen was dissolved in corn oil (20 mg/ml) and administered by gavage at the indicated time points (0.1-0.15 mg tamoxifen/g mouse body weight). Both male and female mice were used in our experiments and randomized into different treatment groups; for adult MI injury, all the mice were randomized into different groups; for DDC, BDL and CCl4 induced liver injury, all the mice were randomized into different groups.

5. Blinding

   Describe whether the investigators were blinded to group allocation during data collection and/or analysis.

   for the adult mice MI injury, BDL or sham operations. the persons who performed the surgery were blinded to the allocation of different experimental.

Note: all studies involving animals and/or human research participants must disclose whether blinding and randomization were used.

Nature Medicine: doi:10.1038/nm.4437

6. Statistical parameters

For all figures and tables that use statistical methods, confirm that the following items are present in relevant figure legends (or in the Methods section if additional space is needed).

n/a	Confirmed
☐	☒ The exact sample size (*n*) for each experimental group/condition, given as a discrete number and unit of measurement (animals, litters, cultures, etc.)
☐	☒ A description of how samples were collected, noting whether measurements were taken from distinct samples or whether the same sample was measured repeatedly
☐	☒ A statement indicating how many times each experiment was replicated
☐	☒ The statistical test(s) used and whether they are one- or two-sided (note: only common tests should be described solely by name; more complex techniques should be described in the Methods section)
☐	☒ A description of any assumptions or corrections, such as an adjustment for multiple comparisons
☐	☒ The test results (e.g. *P* values) given as exact values whenever possible and with confidence intervals noted
☐	☒ A clear description of statistics including central tendency (e.g. median, mean) and variation (e.g. standard deviation, interquartile range)
☐	☒ Clearly defined error bars

See the web collection on statistics for biologists for further resources and guidance.

Software

Policy information about availability of computer code

7. Software

Describe the software used to analyze the data in this study.	Graph Pad Prism 5.0 was used for data analysis. Image J and Photoline was used for image analysis of immunofluorescence and histochemistry.

For manuscripts utilizing custom algorithms or software that are central to the paper but not yet described in the published literature, software must be made available to editors and reviewers upon request. We strongly encourage code deposition in a community repository (e.g. GitHub). *Nature Methods* guidance for providing algorithms and software for publication provides further information on this topic.

Materials and reagents

Policy information about availability of materials

8. Materials availability

Indicate whether there are restrictions on availability of unique materials or if these materials are only available for distribution by a for-profit company.	All unique materials are readily available from the authors or from standard commercial resources.

9. Antibodies

Describe the antibodies used and how they were validated for use in the system under study (i.e. assay and species).	We show the antibodies in Online Methods. We included the catalogue number for each commercial antibody used, so more detailed information could be obtained from the companies. In addition, we added the dilution for each antibody in our immunostaining so readers could follow the protocol for staining. The antibodies used were as follows: tdTomato (Rockland, 600-401-379; 1:1,000 dilution), TNNI3 (Abcam, ab56357; 1:100 dilution), CDH5 (R&D, AF1002; 1:100 dilution), PECAM (BD Pharmingen, 553370; 1:500 dilution), αSMA (Sigma, F3777; 1:500 dilution), PDGFRa (eBioscience, 14-1401-81; 1:500 dilution), CK19 (DSHB, TROMA-III; 1:500 dilution), HNF4a (Santa Cruz, sc-6556; 1:100 dilution), GFP (Abcam, ab6662; 1:100 dilution).

Nature Medicine: doi:10.1038/nm.4437

10. Eukaryotic cell lines

a. State the source of each eukaryotic cell line used.

No cell line were used

b. Describe the method of cell line authentication used.

No cell line were used

c. Report whether the cell lines were tested for mycoplasma contamination.

No cell line were used

d. If any of the cell lines used are listed in the database of commonly misidentified cell lines maintained by ICLAC, provide a scientific rationale for their use.

No cell line were used

Animals and human research participants

Policy information about studies involving animals; when reporting animal research, follow the ARRIVE guidelines

11. Description of research animals

Provide details on animals and/or animal-derived materials used in the study.

We used C57BL/6J;ICR mixed background mice in our study and noted in the Methods section: Mice. CAG-Dre, ACTB-Cre, UBC-CreER, MHC-MerCreMer, Kit-CreER, R26-loxP-tdTomato, R26-rox-tdTomato, R26-GFP mouse lines were reported previously(12,20,39–43). The IR1, IR2, NR1, NR2, CAG-DreER, Tnni3-Dre, Tnnt2-Dre, Alb-CreER, CK19-Dre and Alb-DreER mouse lines were generated by Shanghai Model Organisms Center, Inc. (SMOC). The IR3 and IR4 mouse lines were generated by the Nanjing Biomedical Research Institution of Nanjing University, Nanjing, China. Sox9-CreER was generated by National Institute for Biological Sciences, Beijing, China. Detailed information could also be obtained in Mice section in Methods.

Policy information about studies involving human research participants

12. Description of human research participants

Describe the covariate-relevant population characteristics of the human research participants.

This study did not involve human subjects.

Nature Medicine: doi:10.1038/nm.4437